Available online at www.sciencedirect.com
SCIENCE DIRECT
Polymer 46 (2005) 6947–6958
polymer
www.elsevier.com/locate/polymer

Thermal degradation of ethylene–vinyl acetate coplymer nanocomposites

Marius C. Costache, David D. Jiang, Charles A. Wilkie*

Department of Chemistry, Marquette University, P.O. Box 1881, Milwaukee, WI 53201, USA

Received 26 April 2005; received in revised form 17 May 2005; accepted 20 May 2005
Available online 20 July 2005

Abstract

The degradation pathway of ethylene–vinyl acetate copolymers and their nanocomposites is investigated using TGA/FT-IR, TGA, GC–MS, cone calorimetry and UV techniques to determine if the presence of the clay has an effect on the degradation pathway. The first step of the degradation, the loss of acetic acid by chain stripping, has been shown to be accelerated by the presence of clay. In this work we show that clay does affect the degradation pathway and that the presence of hydroxyl groups on the edges of the clay could be the cause of the accelerated initial step. The products of the second step of the degradation are changed in quantity and some new products are produced, showing that the clay also has an effect on this step of the degradation pathway. A scheme is suggested to account for the role of the clay in the degradation.

Keywords: Ethylene–vinyl acetate; Fire retardancy; Nanocomposites

1. Introduction

Ever since the Toyota research group developed polyamide/clay nanocomposites [1–3], this class of materials has attracted attention because of their unique combination of enhanced properties [4–6], including improved barrier, mechanical and fire properties. Previous workers have observed enhanced thermal stability, mainly a significant reduction in the peak heat release rate, PHRR, and have suggested two possible mechanisms: a barrier effect due to the clay layers [7] and the and the role of iron in the clay in radical trapping [8]. The barrier effect can be explained by the fact that the clay layers slow mass transfer from the degrading polymer to the vapor phase, thus providing less fuel for the flame, and also insulate the polymer from the heat source.

These mechanisms provide a good explanation for reduction in the peak heat release rate of polymer-layered silicate nanocomposites, but they do not explain why some polymers, notably polystyrene, PS, ethylene–vinyl acetate, EVA, and polyamide-6, PA-6, show large reductions in PHRR while other systems show much smaller effects.

No significant change in the functionalities evolved was observed using TGA–FTIR for polyamide 6 [9]. Previous work from this laboratory has shown that for both polyamide 6 [10] and polystyrene [11] the degradation pathway of the nanocomposite is different from that of the virgin polymer and suggests that the clay traps the degrading polymer and that this trapping permits recombination reactions, which lead to some new products and a change in the amount of the products that are formed.

The thermal degradation of EVA proceeds in two steps. The first is the loss of acetic acid, followed by the degradation of the remaining partially unsaturated polyethylene polymer [12]. Camino et al. [13] observed that acetic acid loss of EVA-clay nanocomposites is accelerated and speculated that this process can be catalyzed by the acidic sites of the nano-dispersed clay. For the second step of EVA degradation, Hussain et al. [14] found as products 1-butene, carbon dioxide, ethylene, methane and carbon monoxide while McGrattan et al. [15] identified hydrocarbons ranging from C_8 to C_{26} grouped in a series of α,ω-dienes, 1-alkenes and *n*-alkanes.

In this study, the possibility that the presence of nano-dispersed clay can change the degradation pathway of EVA is investigated; both the first and second step have been thoroughly studied.

* Corresponding author.
E-mail address: charles.wilkie@marquette.edu (C.A. Wilkie).

0032-3861/$ - see front matter © 2005 Elsevier Ltd. All rights reserved.
doi:10.1016/j.polymer.2005.05.084

2. Experimental

2.1. Materials

The polymers used were Escorene Ultra LD 728 (EVA), a poly(ethylene-*co*-acetate) with 19 wt% vinyl acetate and a melt flow index of 2.0 g/10 min, Escorene Ultra LD 319 (VA content 9%) and Escorene Ultra LD 760 (VA content 28%), all produced and kindly provided by ExxonMobil Co. The inorganic clays used were Montmorillonite (MMT), hectorite (Hect) and magadiite (Mag) in their sodium forms, while the organically modified clays were Cloisite 30B (30B), as well as 30BHect and 30BMag, in which the pristine clays were modified with the same surfactant used for Cloisite 30B (methyl, tallow, bis-2-hydroxyethyl, quaternary ammonium, where tallow is about 65% C_{18}, 30% C_{16}, 5% C_{14}). Montmorillonite was supplied by both Southern Clay Products and Elementis Specialties while Cloisite 30B was provided by Southern Clay Products and hectorite was supplied by Elementis Specialties; the preparation of magadiite has been described by Garces [16].

2.2. Instrumentation

Dispersion of silicates in the polymer matrix was observed by X-ray diffraction measurements (XRD) performed using a Rigaku powder diffractometer with Cu tube source ($\lambda = 1.54$ Å); generator tension was 50 kV at 20 mA. TEM images were obtained at 60 kV with a Zeiss 10c electron microscope; the samples were microtomed using a Richert-Jung Ultra-Cut E microtome. TGA/FTIR was performed in nitrogen, at a flow rate of 60 ml/min and a heating rate of 20 °C/min on a Cahn TG 131 instrument connected to a Mattson Research grade FTIR. The evolved volatile products were sampled at a rate of 40 ml/min, using a 'sniffer' tube that extended to the sample cup. The evolved gases were carried through stainless steel tubing to the IR chamber, the temperature of the tubing and the sample cell was maintained at 250∼300 °C. The sample size is 40∼60 mg and the temperature reproducibility of the TGA is ±3 °C while the fraction of non-volatile is ±3%. Cone calorimeter measurements were performed at an incident flux of 35 kW/m^2, using an Atlas Cone 2 instrument using a cone shaped heater. Exhaust flow rate was 24 L/s and the spark was continued until the sample ignited. The specimens for cone calorimetry were prepared by the compression molding of the sample (about 30 g) into 3× 100 ×100 mm^3 square plaques. Typical results from cone calorimetry are reproducible to within ±10%. GC/MS data were obtained using a Agilent 6850 series GC connected to a Agilent 5973 Series MS (70 eV electron ionization) with temperature programming from 40 to 250 °C. The assignment of peaks utilized coinjection with authentic materials, retention time and analysis of the mass fragmentation patterns. UV spectra were obtained on a Shimadzu UV 2501 instrument and NMR experiments were performed on a 300 MHz Varian spectrometer.

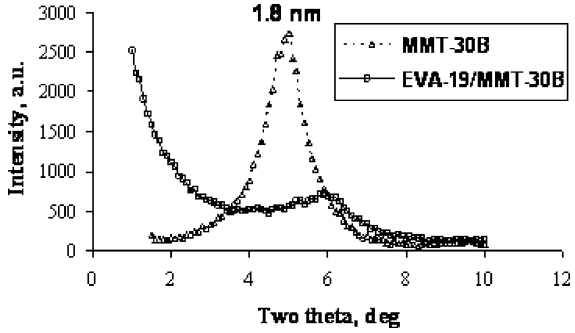

Fig. 1. XRD traces for MMT 30B (dashed line) and EVA/30B (solid line).

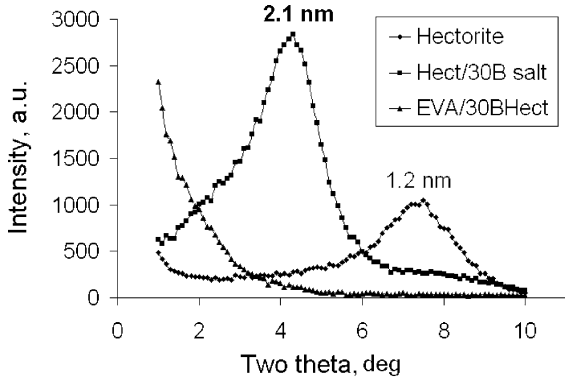

Fig. 2. XRD traces for pristine hectorite, 30BHect and EVA/30BHect.

2.3. Preparation of EVA/clay hybrids

All hybrids were prepared by melt blending the polymer with 3 wt% clay in a Brabender Plasticorder at 120±5 °C, for 20 min at 60 rpm. For the virgin polymer the same melt blending procedure was followed and the samples were used for comparison. The organically modified clays were prepared by cation exchange using a previously described method [8]. The clay in which the hydroxyls were replaced by trimethylsilyl groups was prepared by the reaction of chlorotrimethylsilane with the inorganic clay, as previously described [17]. This clay was then ion-exchanged with the 30B salt (the same surfactant as the one used for organic modification of pristine montmorillonite to afford Cloisite

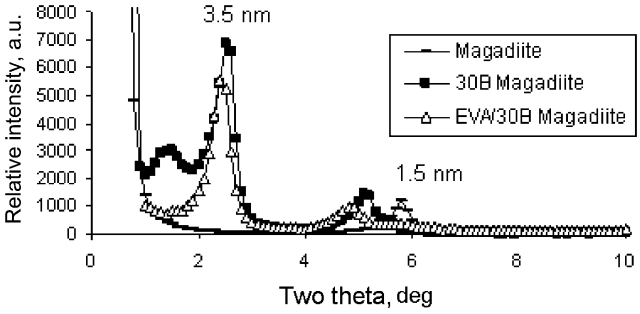

Fig. 3. XRD traces for pristine magadiite, 30BMag and EVA/30BMag.

Table 1
Cone calorimetric data for EVA and its nanocomposites at 35 kW/m^2

Material	t_{ign} (s)	PHRR (kW/m^2)	THR (MJ/m^2)	AMLR (g/s m^2)	ASEA (m^2/kg)
Virgin EVA	73	2303	110	24	430
EVA/30B	70	1174	128	19	670
EVA/30BHect	48	1289	124	18	593
EVA/30BMag	76	2010	98	22	476
EVA/MMT	67	1959	115	23	517

t_{ign}, time to ignition; PHRR, peak heat release rate; THR, total heat release; AMLR, average mass loss rate; ASEA, average specific extinction area, a measure of smoke.

30B clay) to give the organically modified clay, which was used to make the nanocomposite as described above.

3. Results and discussion

3.1. Morphology of EVA/clay hybrids

The X-ray diffraction (XRD) traces of all of the above-mentioned polymer/clay hybrids are shown in Figs. 1–3. The XRD traces of 30B and Hect 30B showed peaks that correspond to a basal spacing of 1.8 and 2.1 nm, respectively. After melt blending with EVA, these peaks all disappear, in agreement with the literature results [13,18]. A small peak is seen in the case of EVA-MMT 30B at 2θ about 6°, which has previously been suggested to arise from unexchanged sodium clay [18]. The exact agreement between the previously reported XRD traces and those shown herein means that these materials can be certainly assigned as delaminated nanocomposites [13,18]. For EVA/30BMag hybrid, the original interlayer spacing of the organoclay (3.5 nm) did not change upon compounding with EVA, as is shown in Fig. 3.

The cone calorimetry results for EVA/30B and EVA/30BHect showed a very large reduction in the peak heat release rate (PHRR), a decrease in the average mass loss rate (AML), an increase in average specific extinction area (ASEA), while the total heat released (THR) was virtually unchanged, which is the expectation for polymer–clay nanocomposites [19]. Previous work from this, and other, laboratories has shown that there is essentially no reduction in PHRR for a microcomposite while there is a good reduction for any system which shows good nano-dispersion [19,20]. The results from EVA/MMT and EVA/30BMagadiite are very similar to those of EVA and this data suggests that the latter two systems are microcomposites while the first two are nanocomposites; all of the results are tabulated in Table 1.

Another indicator of nanocomposite formation is the assertion of Camino that the TGA curves in air and in

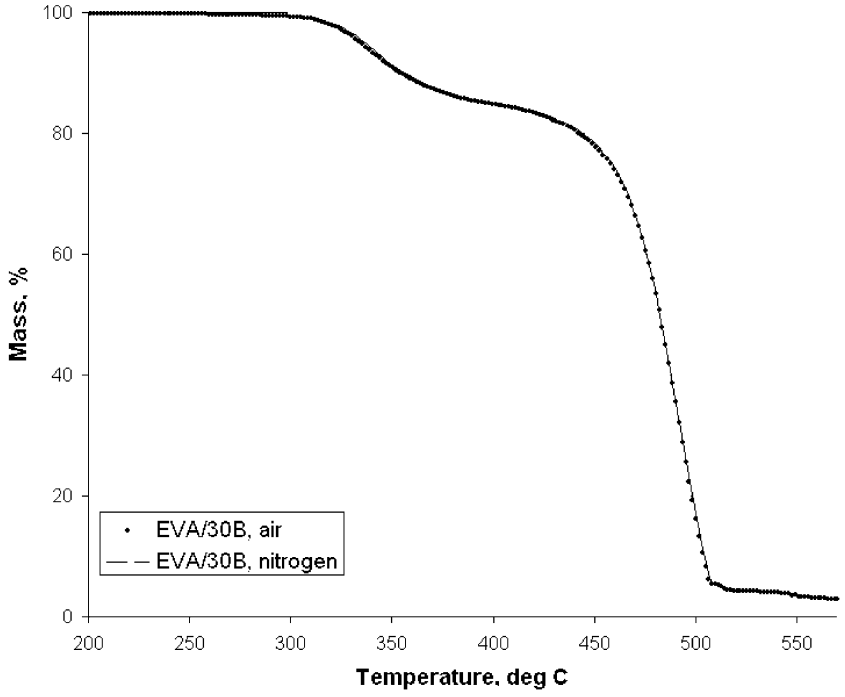

Fig. 4. TGA curves of EVA/30B under air and nitrogen.

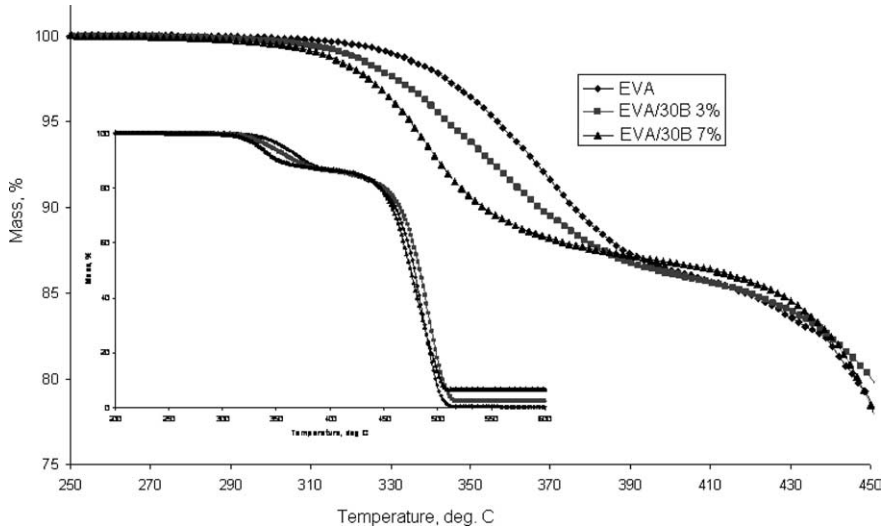

Fig. 5. TGA curves and expansion for EVA and EVA/30B nanocomposites, 3 and 7% clay loadings.

nitrogen are identical for nanocomposites [21]. The TGA curves of the EVA nanocomposite are identical in nitrogen and in air, as shown in Fig. 4. All of this data is in agreement with previous work on EVA and strongly supports the formation of exfoliated nanocomposites for 30B and Hect 30B and a microcomposite for Mag 30B and inorganic MMT.

3.2. First degradation step (acetic acid loss)

The thermal degradation of EVA in nitrogen shows two distinct regions, which have been assigned to the loss of acetic acid and the degradation of the resulting unsaturated material, poly(ethylene-*co*-acetylene), respectively [18]. For the EVA/30B nanocomposites, the loss of acetic acid is accelerated as a function of clay loading, possibly due to catalytic effect of the acidic sites of the clay, as shown in Fig. 5.

If the above mentioned catalytic effect is true, then if the protons on the OH groups on the edges of the clay layers are replaced, one might expect to see no change in the first step of the degradation. It has been shown by Zhao et al. [17] that the hydroxyl groups can react with chlorotrimethylsilane to yield a silylated clay. When this reaction was performed, the infrared spectra of the clay, known herein as NaTMS, was identical to that reported by Zhao. The interlayer spacing decreased from 1.2 nm in pristine MMT to 1.1 nm in NaTMS and it was accompanied by a broadening of the XRD peak, as shown in Fig. 6. The loss of OH groups decreases the overall negative charge of the MMT clay, thus

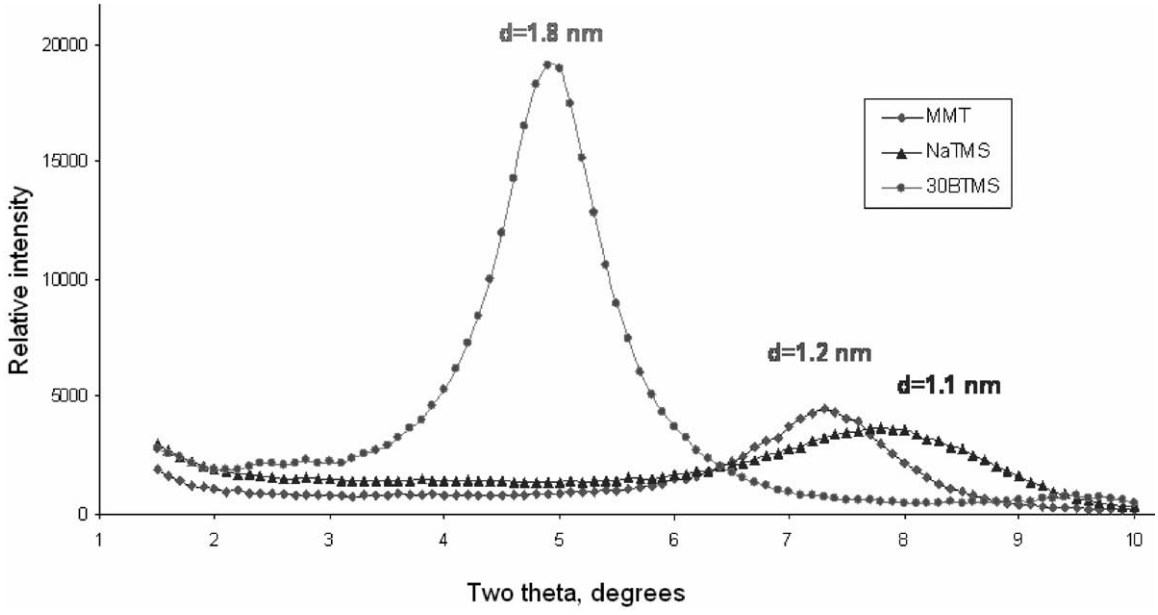

Fig. 6. XRD traces for MMT, NaTMS and 30BTMS.

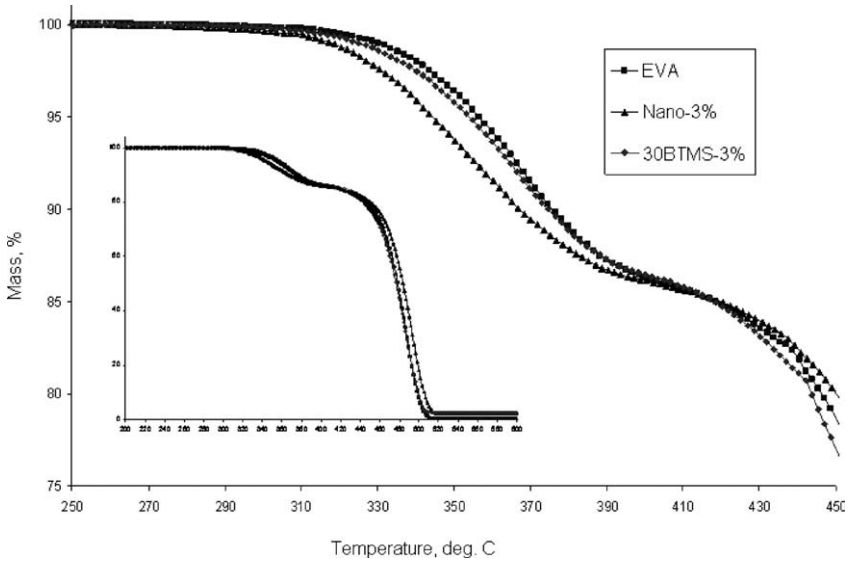

Fig. 7. TGA curves and expansion of EVA, EVA/30B and EVA/30BTMS at 3% clay loading.

reducing its CEC from 90 mmol/100 g to 42 mmol/100 g [17] and this could account for the lower 2θ values observed in NaTMS. The observed broadening may be explained by the non-uniform distribution of the silanol groups within the clay sheets, leading to layer-to-layer variations, which would lead to breadth in the XRD peak, since the values observed are average values. When the sodium cation in NaTMS was exchanged with the 30B cation affording a 30B clay analog (herein named 30BTMS), the interlayer spacing (1.8 nm) is the same as that shown in Fig. 1 for the hydroxy-containing 30B clay.

The TGA behavior of EVA/30BTMS at both 3 and 7% is different from that of the hydroxylated clay and no significant increase in the loss of acetic acid is observed; the TGA curve at 3% clay is shown in Fig. 7. This supports the assertion due to Camino that acetic acid loss is related to the presence of hydroxyl groups on the clay [21].

The transmission electron microscopy (TEM) images of the EVA/silylated clay, at both 3 and 7% clay loading, show relatively poor dispersion of the clay, possibly due to its reduced wetability, and indicate that microcomposites, and not nanocomposites, have been formed (Fig. 8).

3.3. The main degradation step

The evolved gases from virgin EVA and nanocomposites were analyzed using TGA/FTIR. The spectra collected were found to be very similar, showing evolution of acetic acid, carbon dioxide and water in the early stages, followed only by hydrocarbons, as shown in Fig. 9.

Upon expansion, the carbon-hydrogen stretching region shows slight differences. In the case of virgin EVA, a relative intense absorption band at 3085 cm^{-1} can be observed, shown in Fig. 10, corresponding to C–H stretching in 1-alkenes; for the corresponding

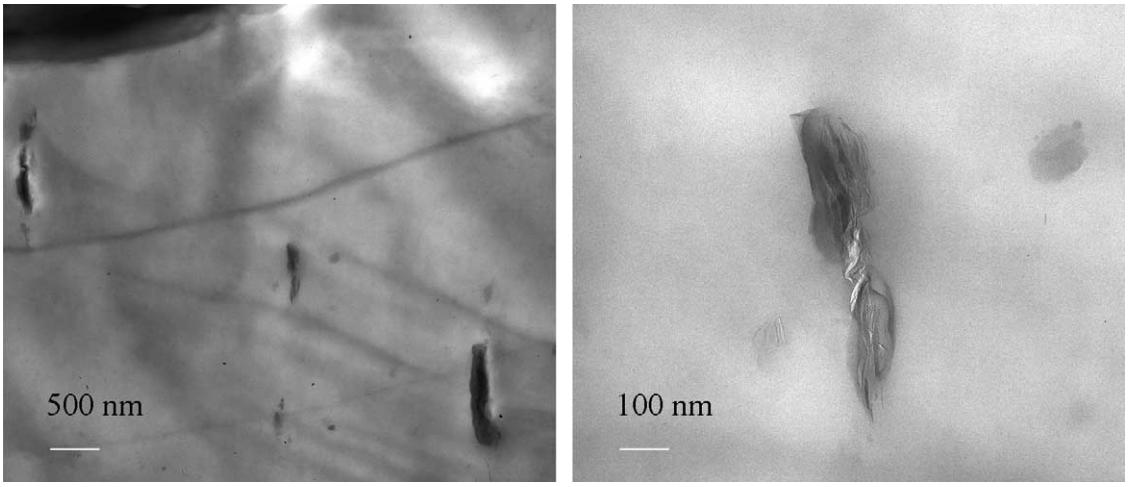

Fig. 8. TEM images of EVA/30BTMS, at low magnification (left) and high magnification (right), for 3% clay loading.

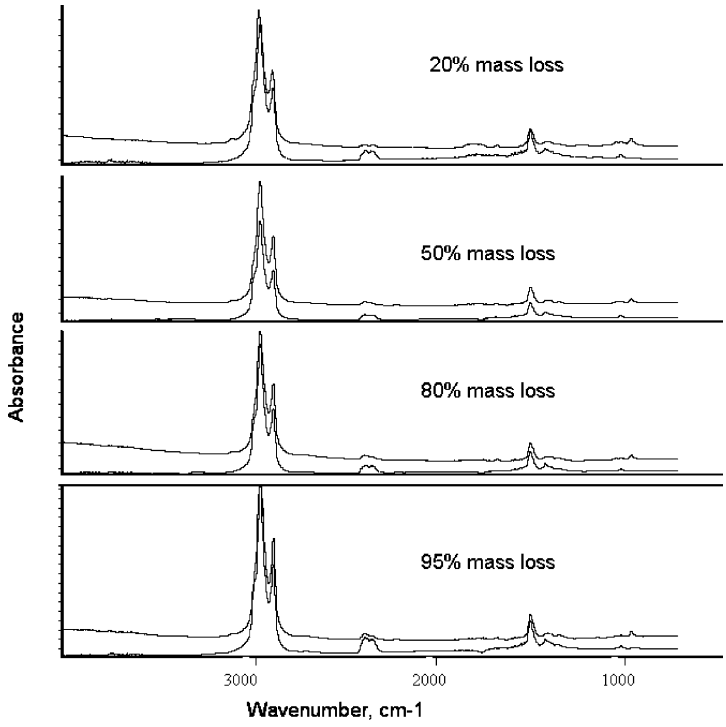

Fig. 9. FTIR spectra of EVA(top spectra) and EVA/30B nanocomposite (bottom spectra) at 20, 50 80 and 95% mass loss.

nanocomposite, this peak is decreased, suggesting that a smaller amount of 1-alkene is generated.

To more thoroughly characterize these hydrocarbons, the evolved products were collected at −78 °C, using a dry ice/acetone cold trap, dissolved in cyclohexane and then analyzed by GS–MS. Samples of EVA containing 9, 19 and 28% vinyl acetate (VA) were studied and all gave similar GC traces; the single difference was the position of maximum abundance, which shifted towards longer carbon chains as the VA content decreased and longer ethylene units were inserted between the VA units, Fig. 11. This suggests that after the loss of acetic acid, the remaining now unsaturated poly(ethylene-*co*-acetylene) undergoes scission at allylic positions.

For EVA, the GC trace shows 'families' of peaks eluting in sets of three, Fig. 12. Using retention times, mass fragmentation pattern analysis and coinjection with authentic materials, the peaks of each series were identified as

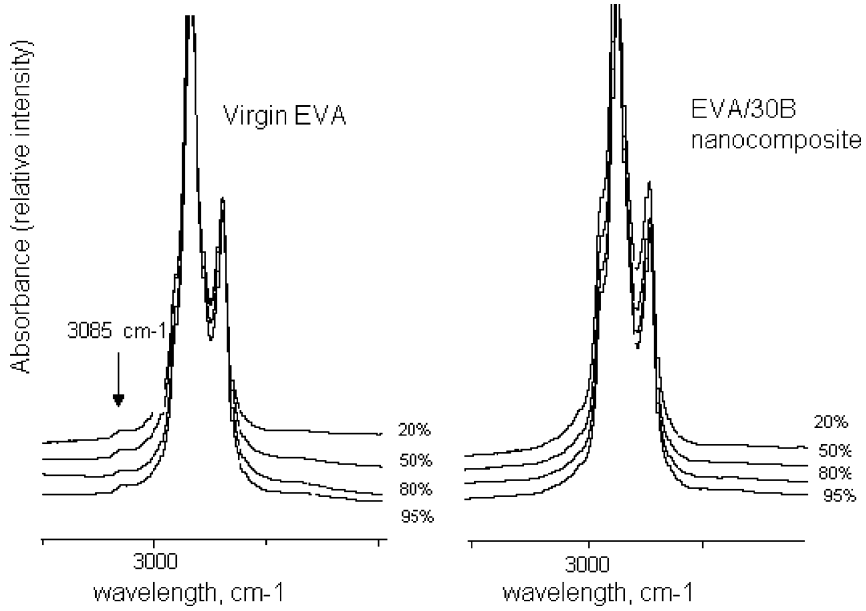

Fig. 10. FTIR spectra expansions of virgin EVA (left) and EVA/30B nanocomposite (right) at 20, 50, 80 and 95% mass loss.

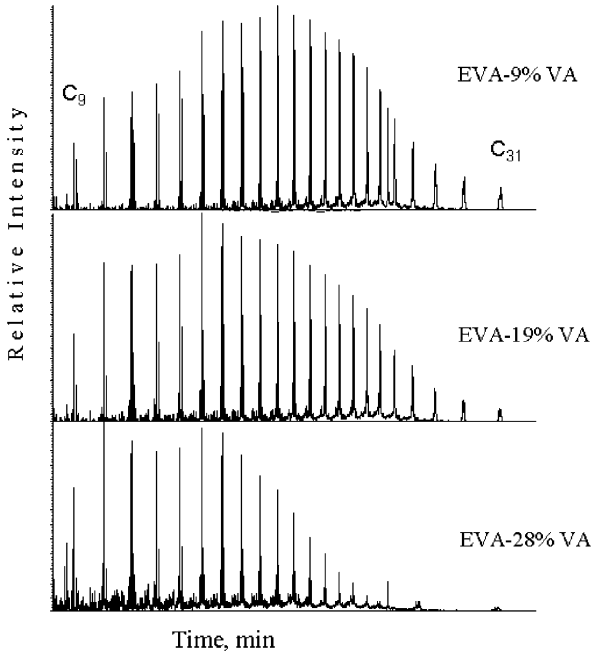

Fig. 11. GC traces from EVA 9, 19 and 28% VA content, respectively.

α,ω-dienes, 1-alkenes and *n*-alkanes, respectively, ranging from C_9 to C_{31}, in accordance with previous work [15].

In contrast, for the EVA/30B nanocomposite, the α,ω-diene peak almost completely disappears, the 1-alkene peaks decreases, and other, new peaks appear, all of which apparently correspond to unsaturated compounds, Fig. 13. The decreased amount of 1-alkene is consistent with the FTIR results. Integration of the three major types of peaks gives a ratio of saturated:unsaturated species of about 27:73 for virgin EVA, which changed to about 43:57 for the nanocomposite. To maintain the hydrogen balance, either additional alkanes must be generated with the formation of polyunsaturated or aromatic species or other unsaturated species containing an internal olefin must be produced at the expense of the terminal olefins. No additional alkanes have been identified either in the final degradation products or in the solid residue at 50% mass loss (by ^{1}H NMR, GC/MS or UV experiments). The other possibility, the generation of internal olefins, is considered more likely and is supported by GC/MS data, in which *cis*-2-olefins and *trans*-2-olefins were identified by coinjection with authentic samples. The other newly generated compounds are believed to be other internal unsaturated species and, to a much smaller extent, cycloalkanes. The presence of nano-dispersed clay platelets can confine the radicals, favoring recombination reactions, as has been shown for polystyrene and polyamide 6 [10,11]. On the other hand, the labyrinth effect due to the clay, delays the evolution of the degradation products thus favoring, along with allylic scission, random scission that could explain the presence of internal alkenes [18].

More insight into nanocomposite degradation can be found from examination of the residue from EVA and its nanocomposite. The degradation was quenched at 50% mass loss and the residue was dissolved in cyclohexane, filtered and analyzed by UV and the spectrum is shown in Fig. 14. The clear solution from EVA showed a single important absorption band, at 245 nm, assigned to isolated carbon-carbon double bonds. On the other hand, the yellow-greenish solution from the nanocomposite showed new

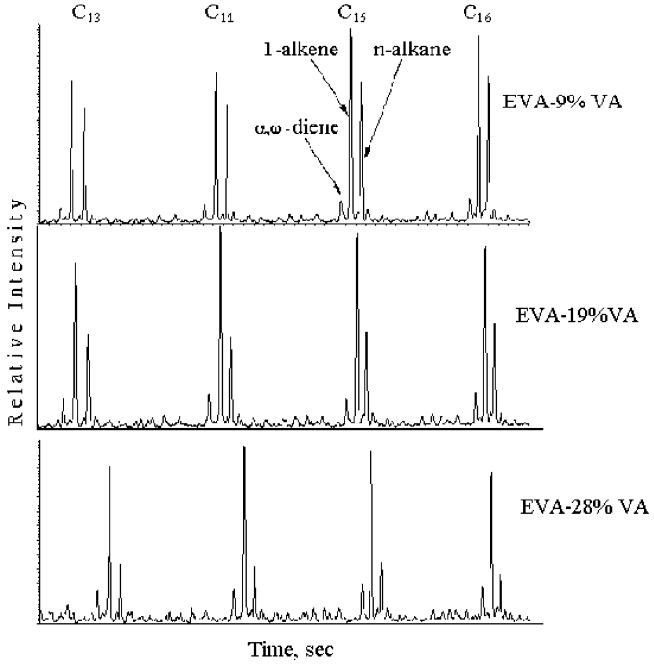

Fig. 12. Expansions of GC traces from EVA 9, 19 and 28% VA content.

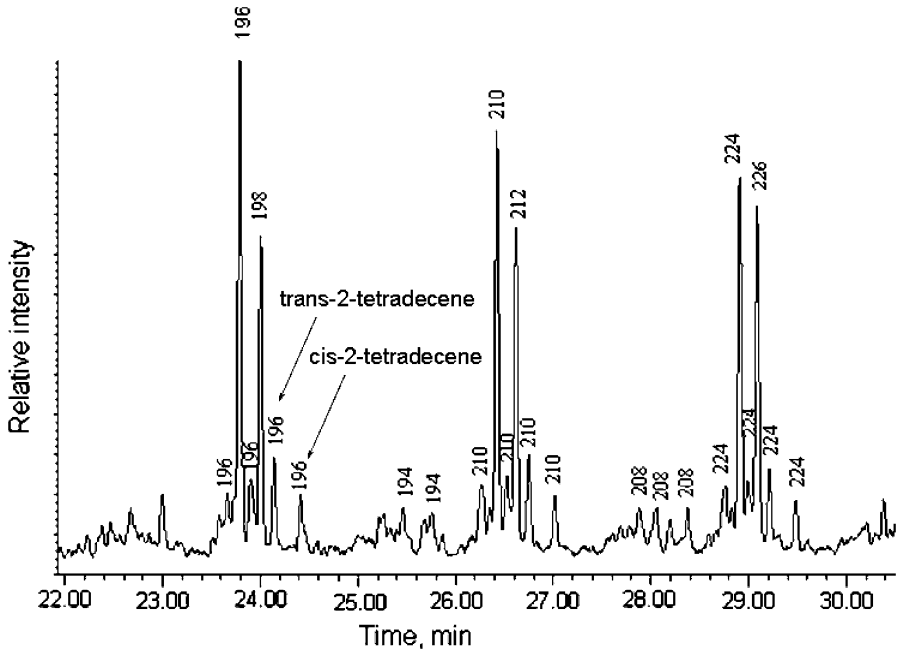

Fig. 13. GC–MS assignments for evolved degradation products from EVA/30B.

absorbance bands at 257, 272 and 289 nm which were tentatively assigned to the presence of various conjugated dienes and/or trienes, based on similar results reported by McNeill [22]. The amount of these latter species is probably not very large since they have not been identified by ^{1}H NMR, but their existence can possibly explain the additional unsaturated compounds found by GC–MS.

To determine if the change in degradation pathway depends upon the nature of the clay, three additional hybrids were studied: EVA/30BHect, EVA/30BMag and a material known to be a microcomposite, EVA/NaMMT. The degraded products were collected using a cold trap and analyzed by GC–MS and selected traces are presented in Fig. 15.

The two nanocomposites gave not only similar, but almost identical results, while the GC traces for EVA, EVA/MMT and EVA/30Mag are the same, but different from that of the nanocomposites. Nano-dispersed clay has an effect on the products and the distribution of the products that are formed in the thermal degradation of EVA

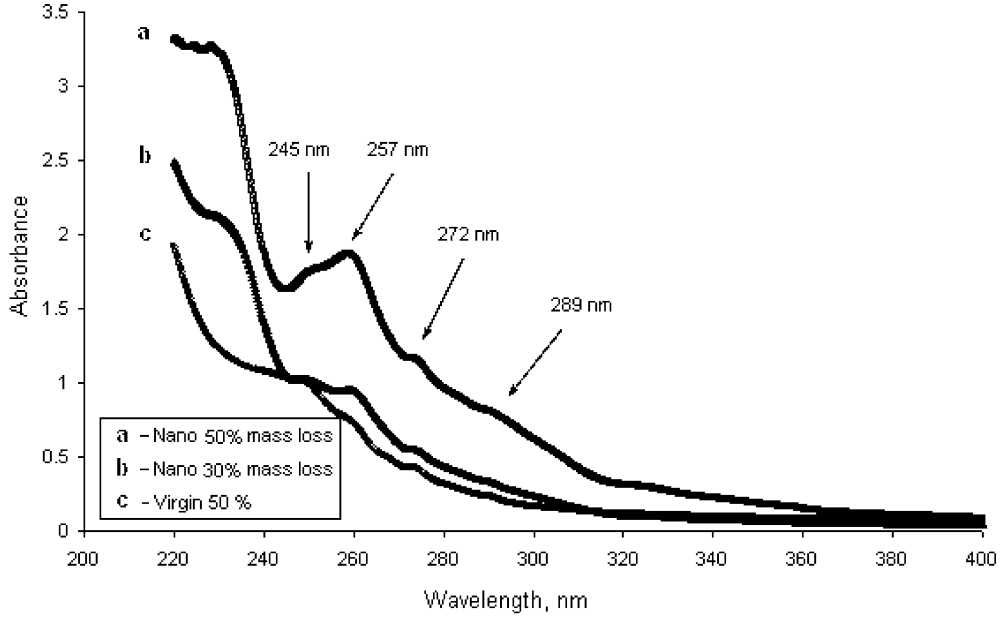

Fig. 14. UV curves for EVA and EVA/30B residue at 50% mass loss.

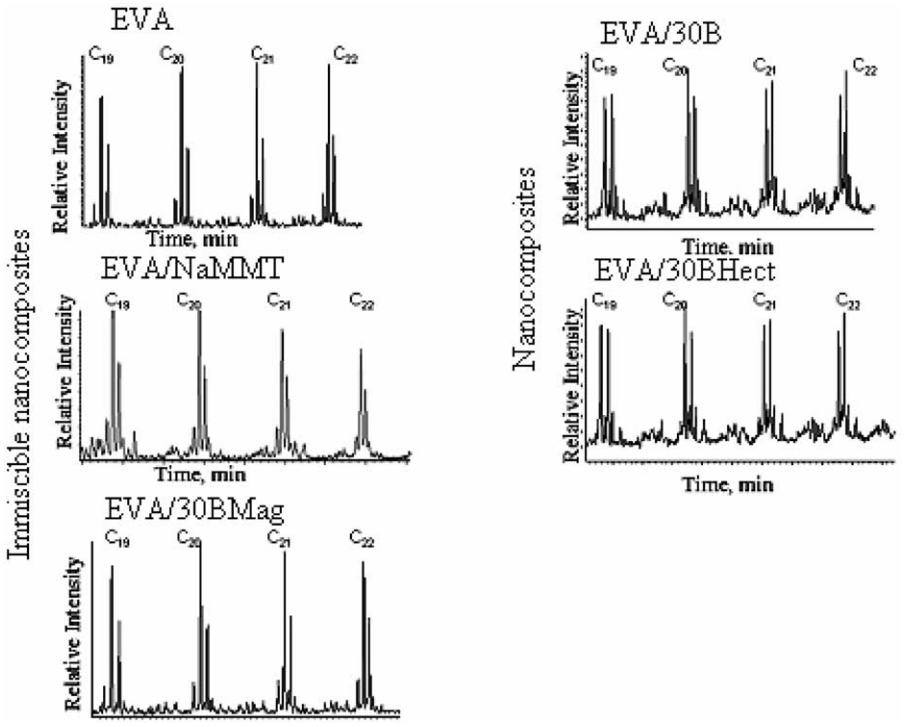

Fig. 15. Expansions of GC traces of virgin EVA, EVA/30B Magadiite, EVA/Na MMT, EVA/30B MMT and EVA/ 30B Hect.

nanocomposites, but there is no effect when the clay is not well dispersed.

Returning to the EVA/silylated clay hybrids, the GC/MS data collected from the condensable products evolved during the degradation of EVA/30BTMS show an intermediate behavior, presenting features characteristic of nanocomposites (the diene peak is reduced and the presence of new peaks between the major ones) and also characteristics of microcomposites (a smaller change in the ratio of alkene/alkanes than is seen for the nanocomposites), as shown in Fig. 16.

A similar result can be seen from cone calorimetric data. The reductions in the peak heat release rate are 25 and 40% for a 30BTMS clay loading of 3 and 7%, respectively. For comparison, in the case of nanocomposite (3% 30B clay loading) the reduction is 50%, while that in a microcomposite

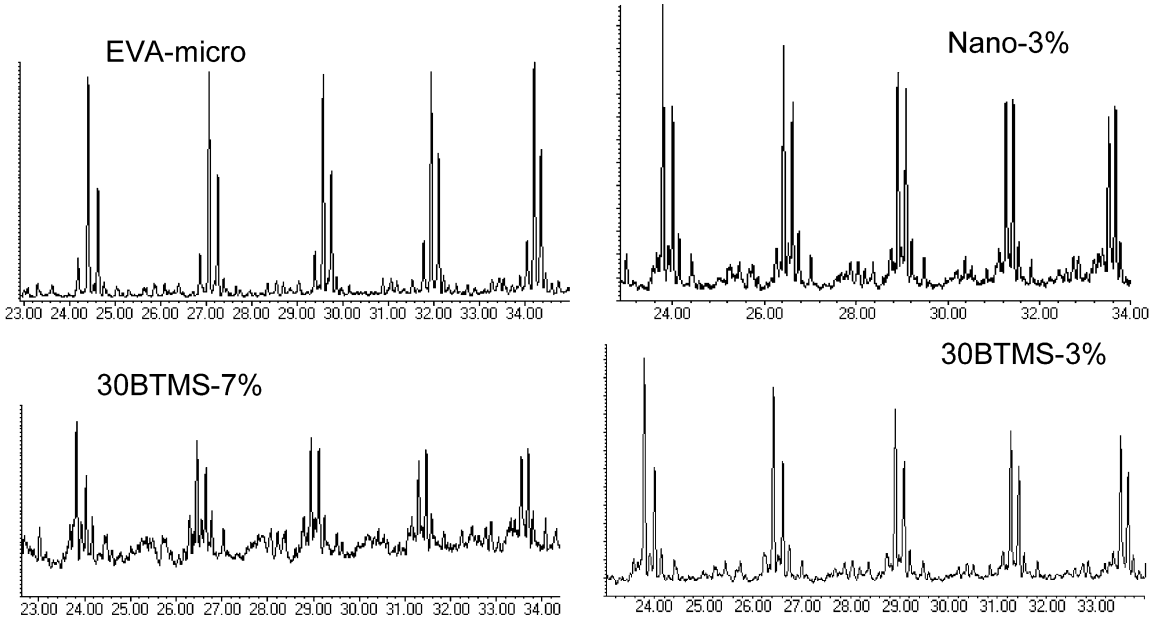

Fig. 16. Selected GS traces, ranging from C_{14} to C_{18}, of microcomposite, nanocomposite and EVA/30BTMS hybrids (3 and 7%).

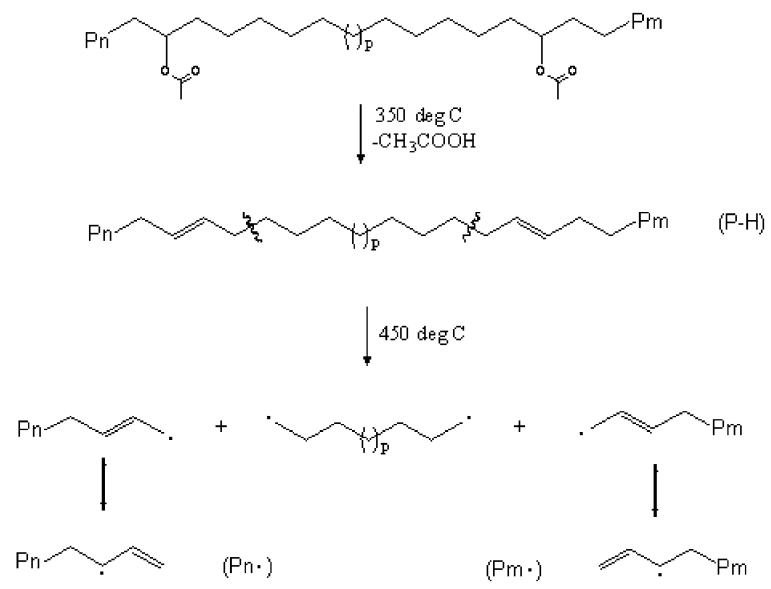

Scheme 1. Thermal degradation of EVA by allylic scission of the main chain.

is 15%. These results suggest that even though the TEM images show only microcomposite formation, some degree of nano-dispersion has been achieved.

Summarizing the results for EVA nanocomposites, a degradation mechanism must address: the prolonged burning time and reduced peak heat release rate (as seen from cone calorimetry), increased thermal stability (as observed from TGA) and the change in the degradation products (reduction of the amount of 1-olefins and formation of other unsaturated species, as seen from GC–MS).

In the initial stage of degradation, upon heating to roughly 350 °C, EVA loses acetic acid, for which some mechanistic aspects have already been presented, resulting in poly(ethylene-*co*-acetylene) having double bonds randomly distributed along the main chain.

At about 450 °C, the latter species undergoes allylic scission, producing diradicals and allylic radicals, which can rearrange into the more stable resonance structure—secondary allylic radicals (Scheme 1).

The diradicals can undergo, at each end, either hydrogen abstraction by radical transfer reactions with the initial polymer, or hydrogen loss by disproportionation. The net result from these reactions, schematically represented in Scheme 2, is the formation of n-alkanes, α,ω-dienes and terminal olefins, already identified by GC–MS (Scheme 2).

Differences in the degradation of the nanocomposite and virgin EVA may arise from secondary reactions which the secondary allylic radicals can undergo. In the case of the nanocomposite, the clay platelets can confine these radicals, so that recombination reactions become much more probable than in the case of virgin EVA (Scheme 3). For virgin EVA, the most probable reactions are radical transfer reactions with the original polymer, from which the newly formed radicals can return to the degradation cycle, undergoing additional scission, etc.

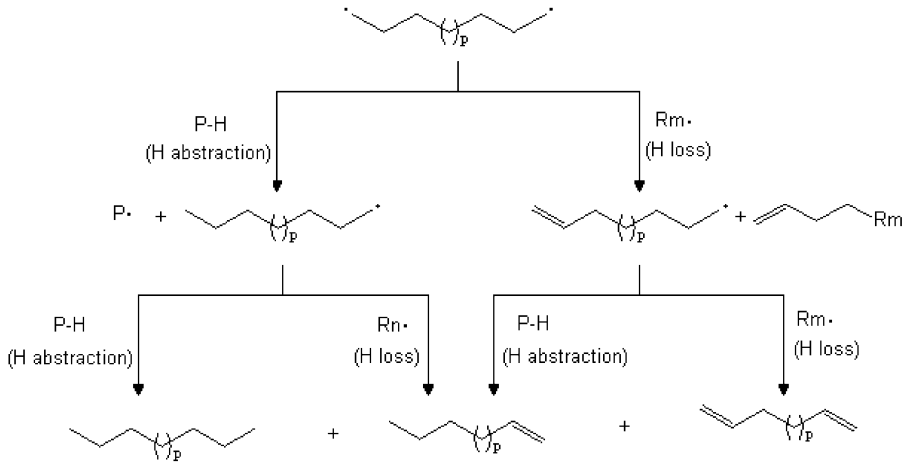

Scheme 2. Further degradation reactions of EVA leading to the formation of alkanes, alkenes and dienes.

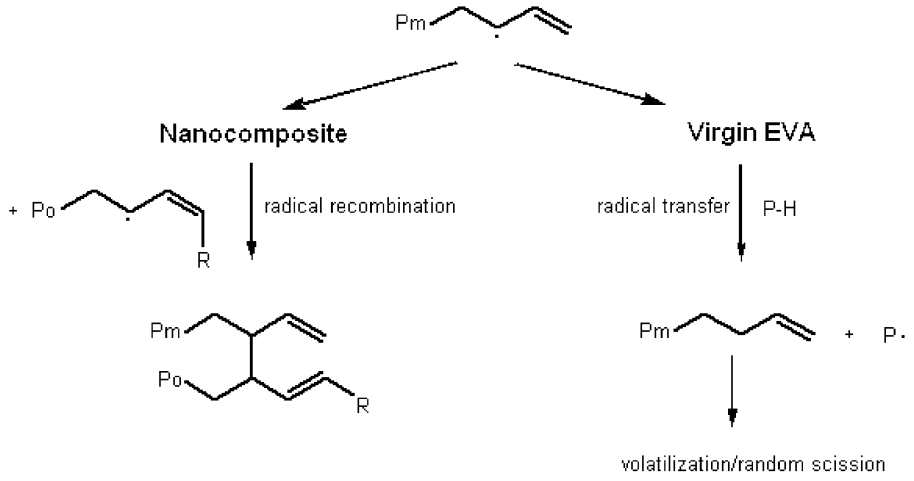

Scheme 3. Possible radical recombination reactions for EVA nanocomposites.

Further, in the case of the nanocomposite, other reactions might take place, favored by the confinement provided by clay platelets and produce (Scheme 4):

- cross-linked structures which can undergo further scission, leading to the formation of radical species which can either disproportionate, leading to the formation of various branched trienes, or recombine, forming other cross-linked structures and/or internal olefins. The presence of internal olefins in the case of nanocomposites can be explained by radical recombination reactions.
- linear polymer chains which have a favorable orientation promoted by clay confinement to undergo transient cross-linking.

In addition, the trienes formed can undergo Diels–Alder cycloaddidion reactions (for which it is well known that clay can act as a catalyst [23]), leading to cyclic structures and possibly, upon hydrogen abstraction, to other unsaturated structures.

All these cross-linked, branched or multiple double bonds containing structures can explain the increased thermal stability of the nanocomposite observed by TGA, since more energy is required to break the additional bonds formed. This could also explain, in conjunction with the

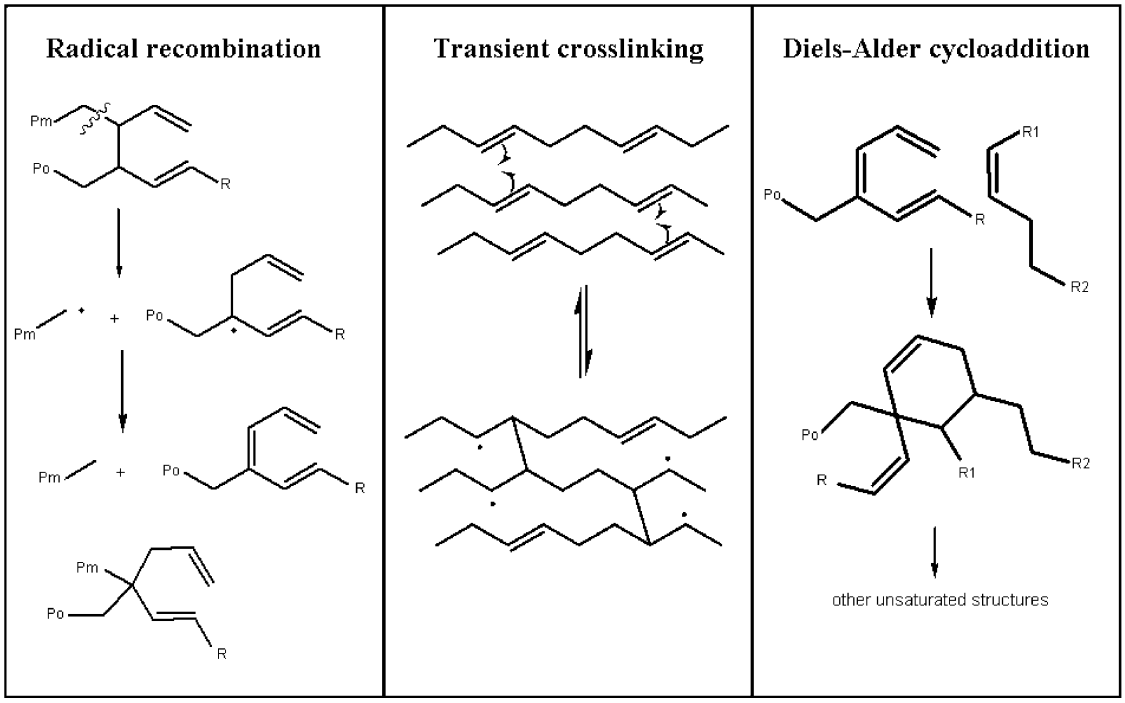

Scheme 4. Secondary reactions in the thermal degradation of EVA nanocomposites.

barrier effect, the prolonged burning time observed in the cone calorimeter and the reduction in the peak heat release rate.

Beyer [24] has studied the chars formed in cone calorimetric experiments by solid state NMR spectroscopy and has shown that an EVA-like material is still present after 200 s of burning of the EVA nanocomposite, supporting the retention of an EVA-like material for a long time period. The NMR peaks of this material are gone after 50 s in the absence of the clay. This observation is entirely in accord with the observations of this paper in which the clay contains the degrading polymer and permits recombination reactions, which will be EVA-like in structure.

4. Conclusions

In the early stages of the EVA degradation, the loss of the acetic acid seems to be catalyzed by the hydroxyl groups present on the edges of the clay. The TGA–FTIR and GC–MS results of thermal degradation of EVA in the presence and in the absence of clay show that even though the two processes are very similar, subtle changes occur, leading to the formation of products that differ both in quantity and identity. It is suggested that these products form as a result of radical recombination reactions that occur because the degrading polymer is contained within the clay layers for a long enough period of time to permit the reactions. The formation of these new products explains the variation in the peak heat release rate that is observed in a cone calorimeter. In cases where there are multiple degradation pathways, the presence of the clay can promote one of these at the expense of another and thus lead to different products and hence a different rate of volatilization.

References

[1] Usuki A, Kojima Y, Kawasumi M, Okada A, Kurauchi T, Kamigaito O. J Mater Res 1993;8:1174–8.
[2] Usuki A, Kojima Y, Kawasumi M, Okada A, Fukushima Y, Kurauchi T, Kamigaito O. J Mater Res 1993;8:1179–84.
[3] Usuki A, Kojima Y, Kawasumi M, Okada A, Fukushima Y, Kurauchi T, Kamigaito O. J Mater Res 1993;8:1185–9.
[4] Okada A, Usuki A. Mater Sci Eng 1995;C3:109–15.
[5] Gianellis EP. Adv Mater 1996;8:29–35.
[6] Alexander M, Dubois P. Mater Sci Eng 2000;R28:1–2.
[7] Gilman JW, Kashiwagi T. In: Pinnavaia TJ, Beall GW, editors. Polymer–clay nanocomposites. New York: Wiley; 2000. p. 193–205.
[8] Zhu J, Uhl FM, Morgan AB, Wilkie CA. Chem Mater 2001;13: 4649–54.
[9] Liu T, Liu Z, He C, Sue HJ. Polym Degrad Stab 2003;81:47–56.
[10] Jang BN, Wilkie CA. Polymer 2005;46:3264–74.
[11] Jang BN, Wilkie CA. Polymer 2005;46:2933–42.
[12] Camino G, Sgobbi R, Colombier C, Scelza C. Fire Mater 2000;24: 85–90.
[13] Riva A, Zanetti M, Braglia M, Camino G, Falqui L. Polym Degrad Stab 2002;77:299–304.
[14] Maurin MB, Dittert LW, Hussain AA. Thermochim Acta 1991;186: 97–102.
[15] McGrattan BJ. Appl Spectrosc 1994;48:1472–6.
[16] Garces, JM, Lakso, SR, Schoeman, BJ, Ulmer, DC. Patent Application WO 1/83370 A2.
[17] Zhao C, Feng M, Fangling F, Qin H, Yang M. J Appl Polym Sci 2004; 93:676–80.
[18] Zanetti M, Kashiwagi T, Falqui L, Camino G. Chem Mater 2002;14: 881–7.
[19] Gilman JW, Kashiwagi T, Nyden M, Brown JET, Jackson CL, Lomakin S, et al. In: Al-Maliaka S, Golovoy A, Wilkie CA, editors. Chemistry and technology of polymer additives. London: Blackwell Scientific; 1998. p. 249–65.
[20] Zhu J, Start P, Mauritz KA, Wilkie CA. Polym Degrad Stab 2002;77: 253–8.
[21] Zanetti M, Camino G, Thomann R, Mulhaupt R. Polymer 2000;42: 4501–7.
[22] Gardner DL, McNeill IC. J Therm Anal 1969;1:389–402.
[23] Adams JM. Appl Clay Sci 1987;2:309–42.
[24] Beyer G. J Fire Sci 2005;23:75–87.